

DOUBLE ELECTRIC LAYER IN THE STATIONARY SHOCK WAVE STRUCTURES OF A SUPERSONIC FLOW

D. Janette Drake

ADVISOR: L. Vušković

Department of Physics
Old Dominion University
4600 Elkhorn Ave, Norfolk, VA 23529

One of the most challenging issues facing NASA's Mars exploration probes is the interaction between the acoustic shock waves formed during entry and the plasma created due to the friction between the probe and the atmosphere. This interaction can manifest itself in the form of a localized increase of electron temperature, plasma induced shock dispersion and acceleration, optical emission enhancement, or double electric layers. We are performing experimental modeling on simulated Martian atmospheric entry plasma along with an Ar/H₂/Air discharge as an example. Characterization of the supersonic flowing discharges is carried out to understand the effects of gas heating in the discharge and the associated effects due to drift of the excited species. Special emphasis is given to the effects of adding H₂ to an Ar discharge and adding air to an Ar/H₂ discharge. In addition, a comparison is made between the two types of discharges.

Introduction

NASA's Mars exploration missions seek to understand Mars as a dynamic system, including understanding of the potential habitability of the planet and the structure of the atmosphere. To explore the planet, NASA has sent various Martian landers to observe the climate changes in the atmosphere, measure temperature changes at different altitudes above the surface, and look for water below the planet's surface.

One of the most challenging phases the landers face is the atmospheric entry phase. During this phase the friction between the atmosphere and the landers will cause thermal ionization of the surrounding gas. In addition, a shock wave will form just in front of the probe due to the high velocity at which these landers enter. The interaction between this shock wave and the plasma formed around the probe can manifest itself in the form of a

localized increase of electron temperature, plasma induced shock dispersion and acceleration, optical emission enhancement, or a double electric layer.¹ Many experiments have been performed in recent years to study these effects more indepthly.

A number of these experiments^{2,3} have observed the effects of temperature on the shock wave in a weakly ionized gas. In addition, these experiments observed a localized increase of the electron temperature at the shock fronts and the dispersion of these shocks along the axis of symmetry of the discharge.⁴ Additional experiments^{5,6} have shown the enhancement of the optical emission of excited states at the shock fronts with an excessive increase of radiation from the electronically excited states across the shock layer.

It has been well documented that double electric layers form at shock fronts due to the

separation and redistribution of space charge across the shock layer.^{7,8} So far the formation and structure of the double electric layer has not been studied in the context of planetary entry plasma.

Our primary objective is to study the double electric layer formed by the interaction of Martian atmospheric entry plasma with a shock wave. In order to accomplish this objective, we must first perform detailed measurements of the gas and electron temperatures and the electron density to allow for characterization of the free flowing discharges. Once the discharge has been characterized completely, a blunt body can be added to the discharge to create a shock wave. The interaction should produce the previously described effects stated in Ref [1].

This paper is thus set up as follows: In the following section we discuss the supersonic flowing microwave cavity discharge in a Martian simulated gas and in Ar/H₂/Air,ⁱ which was primarily used for comparison. In the next section, we discuss the characterization of an Ar/H₂/Air discharge with emphasis on the effects of adding H₂ to an Ar discharge and adding air to an Ar/H₂ discharge. In the last section, we describe the current results for the characterization of a Martian simulated gas.

Experimental Approach

The experimental set-up shown in Fig. 1 is a combination of supersonic flow tube and a microwave cavity discharge. Using an evacuated quartz tube as a wave guide, supersonic flow was generated with a cylindrical convergent-divergent (de Laval) nozzle upstream of the cavity. We used a commercial microwave generator operating in

ⁱ In the Ar/H₂/Air mixtures, I am referring to terrestrial air.

TE_{1,1,1} mode to sustain a cylindrical cavity discharge at power density between 0.5 and 4 W/cm³. We used a gas mixture of 95.71% CO₂, 2.75% N₂, and 1.54% Ar for simulations of the Martian atmosphere. In addition, we used Ar with varying amounts of H₂ and air in order to compare results with the Martian atmosphere gas. Teflon spheres of half inch diameter will be placed in the path of the flowing discharge to produce a stationary shock wave.

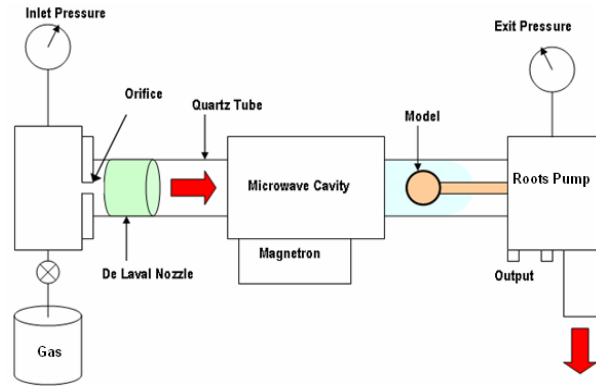


FIG. 1. Scheme of the supersonic flowing experiment.

Through careful measurement of the inlet pressure (p_1) and exit pressure (p_2) in a supersonic Ar flow, we determined the Mach number (M) for our de Laval nozzle from⁹

$$M = \sqrt{2 \frac{\left(\frac{p_1}{p_2}\right)^{\frac{(\gamma-1)}{\gamma}} - 1}{(\gamma-1)}} . \quad (1)$$

Using the specific heat ratio (γ) for the Martian atmosphere of 1.29, we found that $M = 2$. After comparison with the velocity measurements from the Pathfinder, Viking L1 & L2, and MER Opportunity landers, we determined that this was equivalent to an altitude of 10-13 km above the Martian surface. This will assist in the comparison between our experimental simulations and the measurements from the Martian landers.

It has been observed¹⁰ that electronically excited states tend to accumulate at the location of a shock inside a supersonic flowing discharge. As such, we used optical emission spectroscopy as our primary diagnostic tool to observe the spectra of the excited states. In Fig. 2, we show that a CCD camera was used in conjunction with a spectrometer for measurement of the gas and electron temperature. The observed spectral frames were calibrated using a Spectra Physics Pen lamp and the intensity was calibrated using a Newport/Oriel absolute blackbody irradiance source.

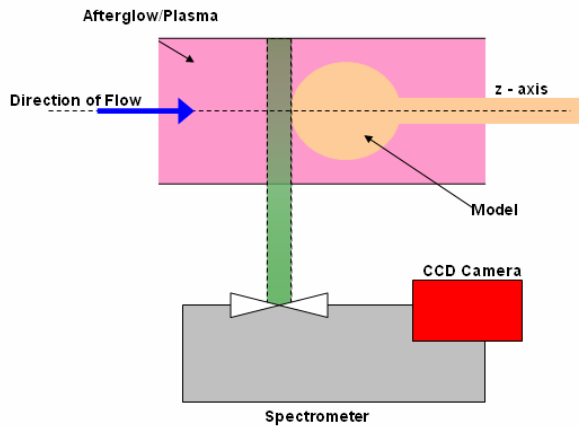


FIG. 2. Optical emission spectroscopy set-up.

We show in Fig. 3 the populations of the observed Ar I states in a free flowing discharge of Ar with 5% H₂ at different applied voltages on the magnetron. We noticed that the populations although higher for the higher voltage, seemed to decrease more rapidly as we go to higher energy levels.

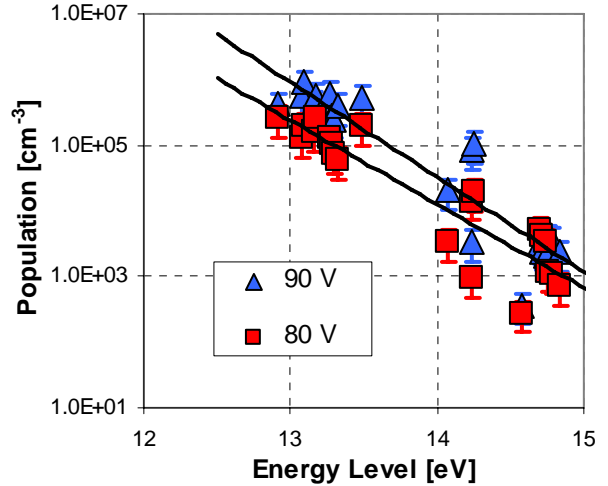


FIG. 3. Population of Ar I states as a function of the energy level.

Experimental Results and Analysis of an Ar/H₂/Air Discharge

In a supersonic flowing discharge the heavy particles have a velocity comparable in magnitude to the thermal velocity. This leads to substantial drift of excited particles downstream of the cavity. In order to account for possible effects caused by drift, we had to determine the rotational, vibrational, and electron temperatures as well as the electron density in the discharge.

Rotational Temperature

We have chosen to use the N₂ C³Π_u – B³Π_g second positive system since it can be identified in an emission spectra and it has a large oscillator strength.¹¹ The rotational spectrum of the N₂ C³Π_u - B³Π_g system consists of three branches: P, Q, and R. Further, the P and R branches are split into three sub-branches, and Q branch is split into two.

To determine the rotational temperature, a Boltzmann distribution for the J' values of the R2 sub-branch was utilized. By measuring the spectral line intensity, $I(J')$, and employing¹²

$$I(J') = \frac{2J'+1}{Q} e^{-J'(J'+1) \frac{hcB_x}{k_B T_R}}, \quad (2)$$

we calculated the rotational temperature. Here Q is a fitted constant, h is Plank's constant, c is the speed of light, B_x is 198.98 m^{-1} , and k_B is the Boltzmann constant.

We observed the changes in the rotational temperature for a given amount of H_2 in the discharge as function of the amount of air in the discharge. Results are presented in Fig. 4. We found that the rotational temperature decreases by increasing both H_2 and air. The data converges to a value of about 900 K which is the average rotational temperature in pure air under the same conditions.

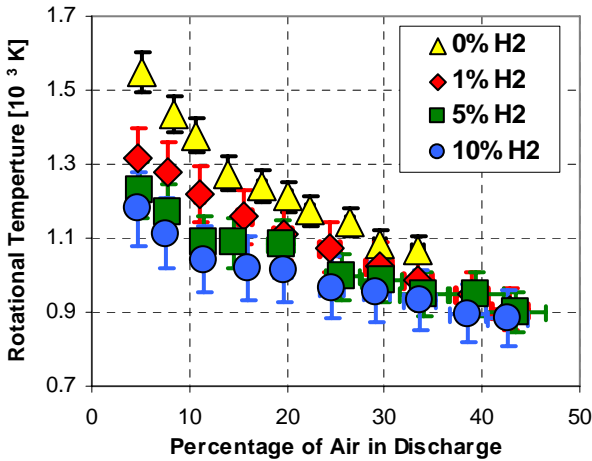


FIG. 4. Rotational temperature as a function of the percentage of air in the discharge.

In order to obtain information about the overall power balance in the discharge, we took measurements of the rotational temperature in the Ar/H_2 discharge as a function of the applied voltage on the magnetron and present these results in Fig. 5. We found that the rotational temperature decreased with the higher applied voltages. At around 90 V the rotational temperature reaches a minimum.

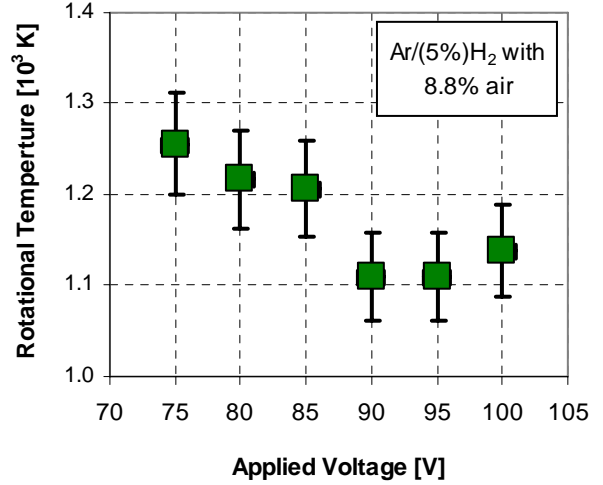


FIG. 5. Rotational temperature as a function of the applied voltage on the magnetron.

Vibrational Temperature

As in the case of the rotational temperature, to determine the vibrational temperature, T_v , we assumed a Boltzmann distribution of the spectral line intensity (I) for the N_2 $\Delta = 2$ vibrational system,

$$I = C_1 A \nu(v') e^{-G(v') \frac{hc}{k_B T_v}}, \quad (3)$$

where C_1 is a fitted constant, A is the Frank-Condon factor, $\nu(v')$ is defined as

$$\nu(v') = \frac{2\pi c}{\lambda}, \quad (4)$$

and $G(v')$ is defined as

$$G(v') = w_e \left(v' + \frac{1}{2} \right) - w_x \left(v' + \frac{1}{2} \right)^2 + w_y \left(v' + \frac{1}{2} \right)^3 + w_z \left(v' + \frac{1}{2} \right)^4. \quad (5)$$

We observed the changes in the vibrational temperature as air and H_2 were added to the discharge, see Fig. 6. As in the case of the rotational temperature, the vibrational temperature decreased with increasing amounts of air in the discharge. However, the

amount of the H_2 had an interesting effect. When 1% H_2 was added to the discharge the vibrational temperature greatly decreased. When 5% H_2 was added, we observed only a slight decrease in the temperature. But when 10% H_2 was added, we saw a large increase in the vibrational temperature.

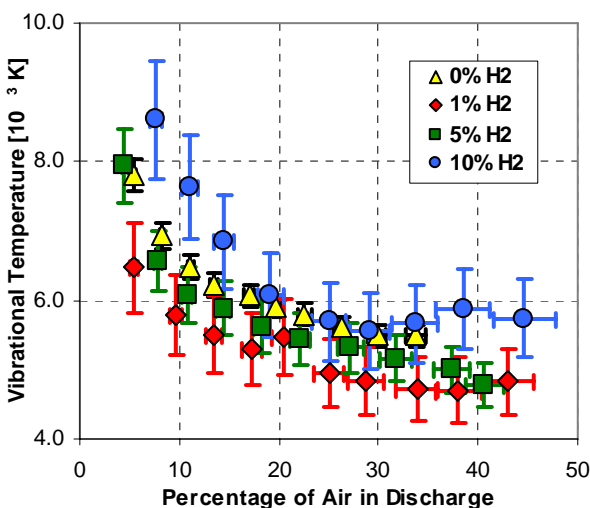


FIG. 6. Vibrational temperature as a function of the percentage of air in the discharge.

Next, we determined the changes in the vibrational temperature as function of the applied voltage on the magnetron and present these results in Fig. 7. We found that, like the rotational temperature, the vibrational temperature decreased with increasing voltage. Then at about 90 V the vibrational temperature became constant with a value of 6000 K.

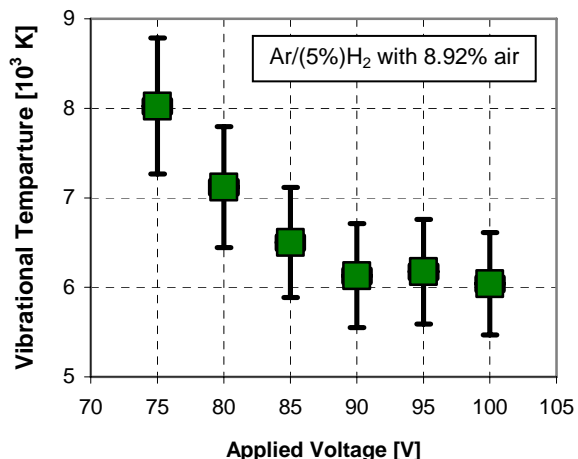


FIG. 7. Vibrational temperature as a function of the applied voltage on the magnetron.

It is evident from Figs. 4 and 6 that the amount of air in the discharge will have a significant effect on the calculated rotational and vibrational temperatures. This change could be due to the fact that as you increase the amount of nitrogen in the system, the number of nitrogen excited species decreases while the number of nitrogen ions increase. To check this assumption we measured the intensity of the N_2^+ ($B^2 \Sigma_u^+$) first negative system. Results in Fig. 8 show an increase in N_2^+ line intensity which indicates an increase in the number of the ions in the discharge.

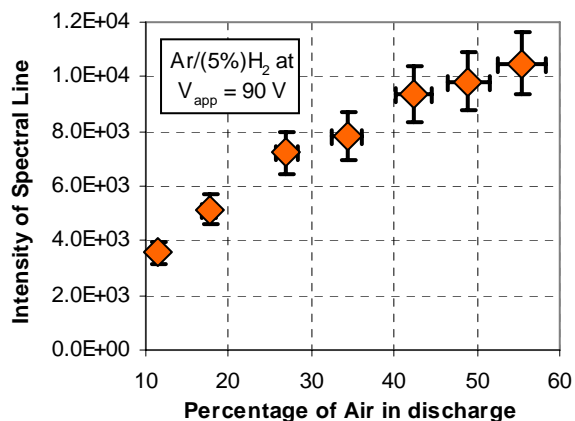


FIG. 8. Intensity of the N_2^+ spectral line as function of the percentage of air in the discharge.

Electron Temperature

By assuming a Boltzmann distribution for the intensities (I_{ki}) of different excited state spectral lines having the same lower level energy and different threshold excitation energies (E_k),¹³ the electron temperature (T_e) can be estimated from

$$I_{ki} = \frac{g_k A_{ki}}{\lambda_{ki}} e^{-E_k/k_B T_e}, \quad (6)$$

where g_k is the statistical weight of the upper level k , A_{ki} is the transition probability, and λ_{ki} is the wavelength.

Results in Fig. 9 show the electron temperature as a function of the applied voltage for a given amount of H₂. The overall effect is that increasing the voltage decreases the electron temperature. This effect is consistent with the results in Fig. 3 which indicated that the electron temperature would be decreasing since the populations of Ar I decreased more rapidly at the higher voltage.

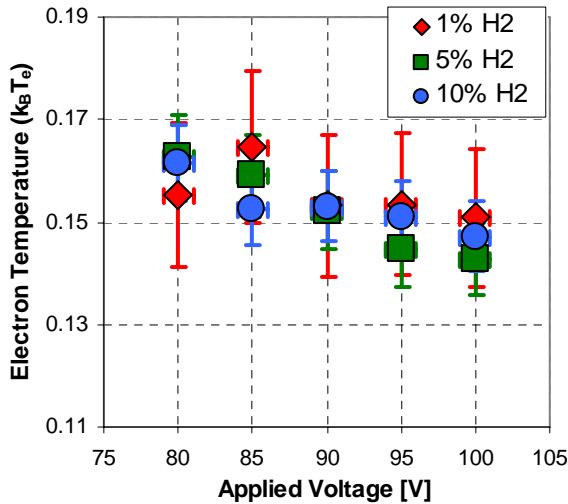


Fig. 9. Electron temperature as a function of the applied voltage on the magnetron.

Electron Density

The electron density was determined from the Stark broadening of H_δ line (410.21nm). The broadening is caused by the interaction of the hydrogen atoms with free electrons in the discharge. A higher electron density will cause a larger line broadening. We evaluated the electron density, N_e , from the empirical formula¹⁴

$$N_e = 8.0 \times 10^{18} \left(\frac{\Delta\lambda_S}{\alpha_{1/2}} \right)^2, \quad (7)$$

where $\alpha_{1/2}$ is 0.150 for H_δ and $\Delta\lambda_S$ is the Stark half-width defined by

$$\Delta\lambda_S = \left(\Delta\lambda_m^{1.4} - \Delta\lambda_{DI}^{1.4} \right)^{1/4}. \quad (8)$$

Here $\Delta\lambda_m$ is the measured half-width and

$$\Delta\lambda_{DI} = \sqrt{\Delta\lambda_D^2 + \Delta\lambda_I^2} \quad (9)$$

where $\Delta\lambda_D$ is the Doppler half-width defined by

$$\Delta\lambda_D = (3.58 \times 10^{-7}) \lambda \sqrt{\frac{T_g}{M}} \quad (10)$$

where λ is the observed wavelength, T_g is the gas temperature, and M is the atomic weight of hydrogen. This procedure includes correction for the instrumental profile through the corresponding half-width $\Delta\lambda_I$.

We observed the changes in the electron density with the applied voltage on the magnetron. Results in Fig. 10 show that the electron density does not vary greatly within the statistical error.

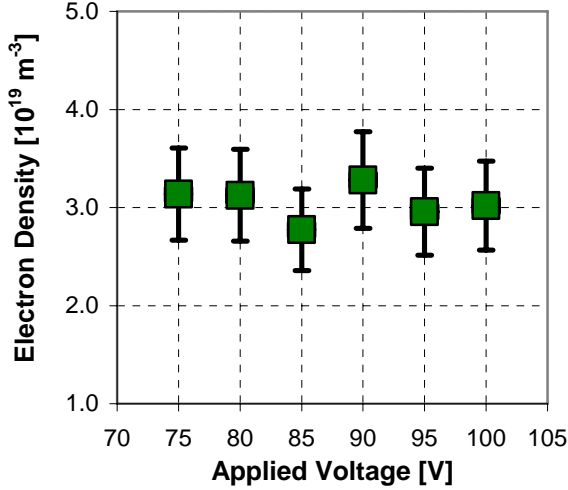


FIG. 10. Electron density as a function of the applied voltage on the magnetron.

Experimental Results and Analysis of a Martian Simulated Discharge

The Martian atmosphere is primarily composed of CO₂ with minor concentrations of N₂ and Ar.¹⁵ Thus we have made a Martian simulated gas consisting of 95.71% CO₂, 2.75% N₂, and 1.54% Ar. As in the case of the Ar/H₂/Air discharge, we must characterize the discharge completely in order to understand the effects that the drift will have on it. We will characterize the discharge by measuring the rotational and electron temperatures and the electron density. Thus far, we have measured only the rotational temperature for the discharge.

Unlike with the Ar/H₂/Air discharge, the concentration of N₂ in the system was very small, which makes observation of the N₂ C³Π_u - B³Π_g rotational bands difficult. We have chosen instead to measure the rotational spectra of the CO Ångstrom system B¹Σ⁺ - A¹Π which is formed in the discharge from the dissociation of CO₂.

By assuming a Boltzmann distribution for the J' values and the intensity $I(J')$ we calculated the rotational temperature by employing¹⁶

$$I(J') = \frac{2C_E v^4}{Q_r} S_{J'} e^{-\frac{B'J'(J'+1)hc}{k_B T_R}}, \quad (11)$$

where C_E is a fitted constant, $v = 19240 \text{ cm}^{-1}$, Q_r is the partition function for all the rotational levels, $S_{J'}$ is the line strength, and $B' = 1.9475 \text{ cm}^{-1}$.

The rotational spectra for CO has three branches: P, Q, and R. The line strength ($S_{J'}$) for each branch can be determined by using the Hönl and London formula.¹⁷ Then by choosing a temperature of 500 K, Eq. (11) can be used to determine how the intensity of each branch will vary with J' . From the calculation presented in Fig. 11, we see that the Q branch has a peak intensity twice as large as the P and R branches.

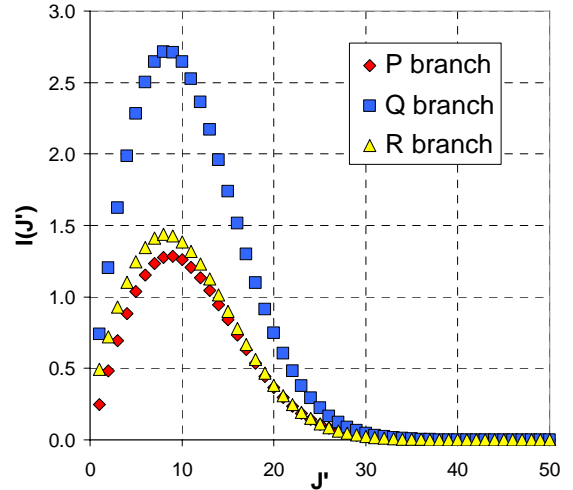


FIG. 11. Intensity of the rotational branches of the CO Ångstrom system at $T_R = 500 \text{ K}$.

Using the line strength of the Q branch, we determined the rotational temperature as function of the applied voltage on the magnetron and presented in Fig. 12. We observed that the rotational temperature reached a maximum at 105 V. In addition, we

see that the rotational temperature is much smaller than that of the Ar/H₂/Air discharge shown in Fig. 4. This is interesting since both discharges contain Ar, N₂, and O₂ but the first discharge contains H₂ while the second has CO₂. The difference in the rotational temperature is therefore attributed to the presence of H₂ in the first discharge and CO₂ in the second discharge.

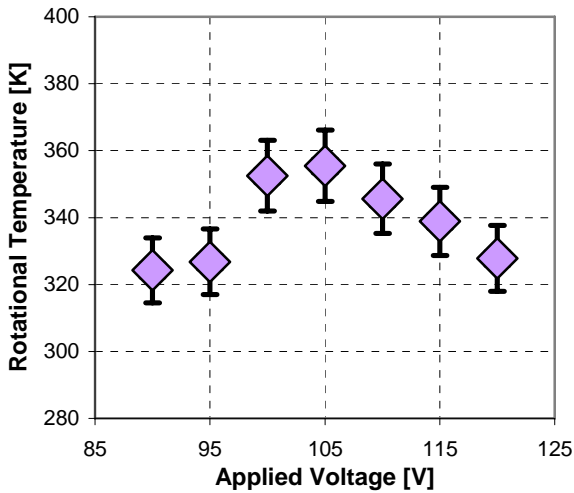


FIG. 12. Rotational temperature as a function of the applied voltage on the magnetron.

Conclusion

In this paper I have discussed the current work we are performing for the characterization of an Ar/H₂/Air discharge and the Martian simulated discharge. We determined the rotational, vibrational, and electron temperature and electron density for an Ar/H₂/Air discharge with varying amounts of H₂ and air. We found through careful analysis of the N₂ and Ar spectra that the rotational temperature and vibrational temperature decrease with increasing amounts of air in the discharge. In addition, we found that the electron temperature decreases slightly with the applied voltage while the electron density appears to be constant.

For the Martian simulated discharge we have determined an appropriate composition for simulations of Martian atmospheric entry plasma. We have also determined the change in the rotational temperature as a function of the applied voltage. We found that the rotational temperature reaches a maximum value when 105 V is applied to the magnetron. We also observed that the rotational temperature in this discharge was much smaller than that of the Ar/H₂/Air discharge.

Now, we will insert the spherical models into the Ar/H₂/Air discharge to observe how each of the previously measured quantities vary across the shock front. According to Ref. [1], we should see an increase in the electron temperature across the shock front. In previous experiments performed in Ar/H₂ discharges¹⁸ we observed an enhancement of the optical emission across the shock front and dispersion of the shock wave. These are all indicators of the double electric layer. By determining the difference in the mean electron temperature across the shock front we will be able to determine the strength of the double layer, since the magnitude of this difference determines the strength of the double electric layer.⁷

For the Martian simulated discharge we will need to determine the electron density and electron temperature along with the physics behind the measured peak in the rotational temperature at 105 V. Then we will have to add the models and observe how these parameters and the rotational temperature change across the shock fronts. We have calculated¹⁹ the electron density and gas temperature across the shock front for the Martian Landers based on the entry data.^{20,21} This will allow for comparison of the electron density in both actual conditions and in our experimental simulations. In addition, we will be able to calculate the concentrations of the species given in the chemical model

developed in Ref. [22]. Since many of the arguments⁴⁻¹⁰ refer to molecular properties of plasma constituents, we will be in a position to compare the results in pure monatomic and in molecular gases.

-
- ¹ S. Popović and L. Vuskovic, *Phys. Plasmas* **6**, 1448 (1999).
 - ² Y. Z. Ionikh, N. V. Chernysheva, A. V. Meshchanov, A. P. Yalin, and R. B. Miles, *Phys. Lett. A* **259**, 387 (1999).
 - ³ A. F. Aleksandrov, N. G. Vidyakin, V. A. Lakutin, M. G. Skvortsov, I. B. Timofeev, and V. A. Chernikov, *Sov. Phys. Tech. Phys.* **31**, 468 (1986).
 - ⁴ S. O. Macheret, Y. Z. Ionikh, N. V. Chernysheva, A. P. Yalin, L. Martinelli, and R. B. Miles, *Phys. Fluids* **13**, 2693 (2001).
 - ⁵ P. Bletzinger, B. N. Ganguly, and A. Garscadden, *Phys. Plasmas* **7**, 4341 (2000).
 - ⁶ D. J. Drake, B. Rodgers, S. Popovic, and L. Vuskovic, *Structure of Stationary Shock Waves in a Weakly Ionized Gas*, 60th Annual Gaseous Electronics Conference, Washington, D.C., October 2007. *Bull. Am. Phys. Soc.* **52**, 62 (2007).
 - ⁷ P. Bletzinger, B. N. Ganguly, and A. Garscadden, *Phys. Rev. E* **67**, 047401(4) (2003).
 - ⁸ N. S. Siefert, AIAA 2006-3572, June 2006.
 - ⁹ J. D. Anderson, *Modern Compressible Flow*, McGraw Hill, Boston, 2003.
 - ¹⁰ P. Bletzinger, B. N. Ganguly, D. Van Wie, and A. Garscadden, *J. Phys. D: App. Phys.* **38**, R33 (2005).
 - ¹¹ J. M. Williamson, P. Bletzinger, and B. N. Ganguly, *J. Phys. D: Appl. Phys.* **37**, 1658 (2004).
 - ¹² G. Hartmann and P. C. Johnson, *J. Phys B: Atom. Molec. Phys.* **11**, 1597 (1978).
 - ¹³ A. Qayyum, S. Zeb, M. A. Naveed, N. U. Rehman, S. A. Ghauri, and M. Zakaullah, *J. Quantitative Spect. Radiative Trans.* **107**, 361 (2007).
 - ¹⁴ M. Ivković, S. Jovicević, and N. Konjević, *Spectrochim. Acta B* **59**, 591 (2004).
 - ¹⁵ R. G. Prinn and B. Fegley, *Ann. Rev. Earth Planet. Sci.* **15**, 171 (1987).
 - ¹⁶ G. Herzberg, *Molecular Spectra and Molecular Structure: Spectra of Diatomic Molecules*, D. Van Nostrand Company, New York, 1950.
 - ¹⁷ H. Hönl and F. London, *Z. Physik* **33**, 803 (1925).
 - ¹⁸ D. J. Drake, "Double Electric Layer in the Stationary Shock Wave Structures of a Supersonic Flow," Virginia Space Grant Consortium's Student Research Conference Program, Williamsburg, VA, April 2007.

-
- ¹⁹ D. J. Drake, S. Popović, L. Vušković, and T. Dinh, "Kinetic modeling of Martian atmospheric entry plasma," to be submitted to the *Journal of Geophysical Research* (2008).
 - ²⁰ A. O. Nier, W. B. Hanson, M. B. McElroy, A. Alvin, and N. W. Spencer *Icarus* **16**, 74 (1972).
 - ²¹ J. T. Schofield, J. R. Barnes, D. Crisp, R. M. Haberle, S. Larsen, J. A. Magalhaes, J. R. Murphy, A. Seiff, and G. Wilson, *Science* **278**, 1752 (1997).
 - ²² T. Dinh, *Decomposition of Carbon Dioxide in a Capacitively coupled Radio Frequency Discharge*, Doctoral Dissertation (Old Dominion University, 2002).